Inorganic Chemistry

Article

Cite This: *Inorg. Chem.* 2018, 57, 9354−9363

pubs.acs.org/IC

Facile Axial Ligand Substitution in Linear Mo≡Mo−Ni Complexes

Jill A. Chipman and John F. Berry*

Department of Chemistry, University of Wisconsin, Madison, 1101 University Avenue, Madison, Wisconsin 53706, United States

Supporting Information

ABSTRACT: Clean axial ligand substitution reactions of heterometallic extended metal atom chains (HEMACs) supported by the dpa ligand (dpa = 2,2′-dipyridylamine) have been synthetically challenging due to side reactions that alter the trimetallic core. Following the hypothesis that a heterometallic core containing second-row transition metals would be more robust toward ligand substitution, we report the synthesis of three new heterotrimetallic compounds, $Mo_2Ni(dpa)_4(OTf)_2$ (**1**), $Mo_2Ni(dpa)_4(NCS)_2$ (**2**), and $Mo_2Ni(dpa)_4(NCSe)_2$ (**3**) that are obtained cleanly and in good yield. Compound **1** may be synthesized either directly by reaction of $Ni(OTf)_2$ with $Mo_2(dpa)_4$ (**4**) or indirectly, by reaction of $Mo_2Ni(dpa)_4Cl_2$ (**5**) with 2 equiv of TlOTf. Axial ligand substitution on **1** via solutions containing NaNCS or KNCSe afford **2** or **3**, respectively. X-ray crystal structures of **1**, **2**, and **3** present short Mo−Ni distances of 2.458(8)Å /2.47(1) Å, 2.548(1), and 2.546(1), respectively. Density functional theory (DFT) calculations indicate a 3-center 3-electron σ bonding interaction between the Mo_2 quadruply bonded core and the Ni in both **1** and **2**. These complexes were analyzed by SQUID magnetometry, supporting the presence of a high spin Ni^{2+} center with $S = 1$.

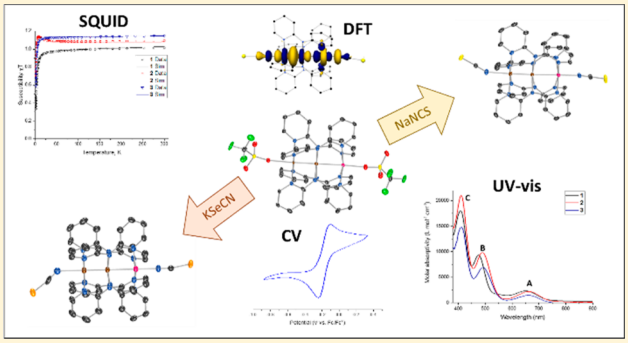

INTRODUCTION

Heterometallic extended metal atom chains (HEMACs) supported by the dpa ligand (dpa = 2,2′-dipyridylamine) were first reported in 2007 independently by us[1] and the group of S.M. Peng.[2] These complexes can be either symmetric of the form $M_A-M_B-M_A$, or unsymmetric with $M_A-M_A-M_B$ structures. Further work in our lab focused on the latter structures has led to the preparation of a large HEMAC family in which M_A is a group VI metal and M_B is either a first or second row transition metal in the +2 oxidation state.[3−10] The overwhelming majority of these compounds feature chloride axial ligands due to the ready availability of MCl_2 starting materials. However, a thorough investigation of the chemical and physical properties of HEMACs requires the discovery of new complexes with variable axial ligands. Homometallic EMACs have been prepared with axial ligands ranging from other halides, pseudohalides, neutral ligands, and organometallic ligands.[3,11−17] These modifications have enabled the tuning of electronic, photophysical, and magnetic properties as well as the formation of one-dimensional polymeric chains via molecular linkers.[18−20]

We have examined substitution of axial chloride ligands in $M_A≡M_A-M_B$ compounds with M_A= Cr and M_B = Mn, Fe, and Co.[21,22] In these past efforts, the substitution reactions have been hampered by poor yields and/or demetalation of M_B upon introduction of the incoming ligand. It was hypothesized that an excess of the substituting axial ligand, which is needed to achieve useful ligand substitution rates of chloride compounds may be leading to demetalation.

To counter this problem, we have examined adding stoichiometric equivalents of the incoming ligand to complexes featuring labile axial ligands. We experienced some success with these methods,[21,22] particularly when labile axial acetonitrile ligands were used. However, the yields of ligand substitution were inconsistent. Another problem surprised us when we examined the products of ligand substitution of Cr≡Cr−Fe compounds. In addition to the expected Cr≡Cr−Fe products, there was a small amount of Cr≡Cr−Cr impurity, indicating that metal atom substitution also occurs under these conditions.[22]

In this work, we set out to explore whether cleaner axial ligand substitution chemistry can be achieved by switching from $Cr≡Cr-M_B$ chains to $Mo≡Mo-M_B$ ones. The strength of the Mo≡Mo quadruple bond was anticipated to prevent the metal atom scrambling issue that we have previously encountered with Cr≡Cr chains. Our recent report of the one-electron oxidized $[Mo_2Ni(dpa)_4Cl_2]^+$ ion[9] provides further support for this hypothesis as moving to a Mo_2 core allowed for the synthesis, isolation, and characterization of this meta-stable complex. In addition, Peng and co-workers have recently reported the preparation of $Mo_2Ni(dpa)_4(NCS)_2$ via a high temperature self-assembly method, which further supports the idea that the Mo_2 complexes are seemingly more robust.[23,24] Herein, we report that the use of a $Mo≡Mo-M_B$ chain does allow for straightforward axial ligand substitution

Received: May 15, 2018
Published: July 19, 2018

DOI: 10.1021/acs.inorgchem.8b01331
Inorg. Chem. 2018, 57, 9354−9363

chemistry to be achieved. Specifically, we report here a systematic series of $Mo_2Ni(dpa)_4X_2$ complexes where X = OTf, NCS, and NCSe. This series allows us to enumerate trends in electronic structure and heterometallic bonding as a function of the axial ligand, X.

RESULTS AND DISCUSSION

Synthesis. In this work, $Mo_2(dpa)_4$ (**4**) is the key precursor used for the preparation of Mo_2Ni chain complexes. In previous work, **4** was prepared by deprotonation of Hdpa with methyllithium followed by reaction with $Mo_2(OAc)_4$.[1] We report here a modified synthetic procedure for **4** that obviates the need for methyllithium. In this new procedure, the salt Kdpa is prepared and isolated through reaction of $KN(tms)_2$ and Hdpa in ether at room temperature at yields exceeding 80% (tms = trimethylsilyl). This salt was characterized via ^1H and ^{13}C NMR spectroscopy and elemental analysis confirms its identity. When Kdpa is allowed to react with $Mo_2(OAc)_4$ in refluxing THF, the resulting $Mo_2(dpa)_4$ is identical by IR spectroscopy to that prepared via the traditional route but is typically obtained in higher yields, greater than 80%.

From **4**, $Mo_2Ni(dpa)_4(OTf)_2$ (**1**) may be directly synthesized. Reaction of **4** with 1.5 equiv of $Ni(OTf)_2$ in molten naphthalene at 225 °C for 2 h affords **1** following workup of the reaction mixture. Complex **1** may also be synthesized via the addition of an acetonitrile solution of 2 equiv of TlOTf to a solution of $Mo_2Ni(dpa)_4Cl_2$ (**5**) in a slightly lower yield. In order to achieve axial ligand substitution, yielding complexes **2** and **3**, an acetonitrile solution containing 2 equiv of NaNCS or KNCSe, respectively was added dropwise to a solution of **1** in dry dichloromethane at 0 °C. Both reactions are accompanied by a color change in which the forest green solution of **1** changes to a goldenrod solution of **2** or a brown solution of **3**. Complex **2** may be isolated as a brown powder in 72% yield or as brown crystals in a 45% yield. Complex **3** may be obtained as a crystalline product in 44% yield. This overall synthetic methodology is outlined below in Scheme 1.

In the course of our work, an alternative synthesis of **2** was reported by Peng and co-workers.[23] In this case, $Mo_2(OAc)_4$, Hdpa, $Ni(OAc)\cdot 4H_2O$, and excess NaNCS were heated together in molten naphthalene to afford **2** in 53% yield. We were surprised that **2** could be prepared under such harsh reaction conditions with an excess of NaNCS. To investigate this further, we therefore attempted to prepare **2** by heating **5** with 36 equiv of NaNCS in molten naphthalene. In our hands, this reaction did not yield the expected $Mo_2Ni(dpa)_4(NCS)_2$ product. Instead, we obtained what we believe to be a mixture of $Ni(Hdpa)_2(NCS)_2$ and $Mo_2(dpa)_4$ based on MALDI−TOF mass spectrometery data. Although $Ni(Hdpa)_2(NCS)_2$ has not been previously reported, analogous compounds have been characterized by Hurley and Robinson and these show similar solubility properties to the material we obtain.[25]

Scheme 1. Synthesis of Complexes 2−5

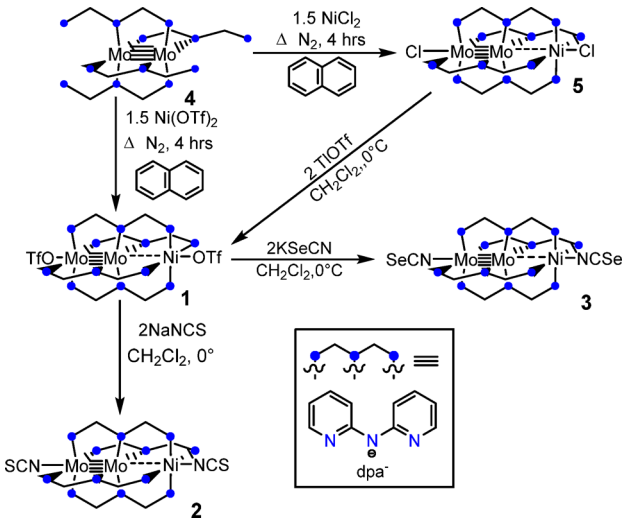

Geometric Features of Synthesized Complexes. X-ray quality crystals of **1**, **2**, and **3** were obtained by layering separate dichloromethane solutions with hexanes (**1**) or diethyl ether (**2** and **3**). Compound **1** crystallizes in the monoclinic space group $P2_1/c$ while **2** crystallizes in the triclinic space group $P\bar{1}$, and **3** crystallizes in the monoclinic space group $C2/c$ (Figure 1.) While **1** presents positional metal atom disorder within the Mo≡Mo−Ni chain, **2** and **3** do not present this disorder. These three structures are fairly similar

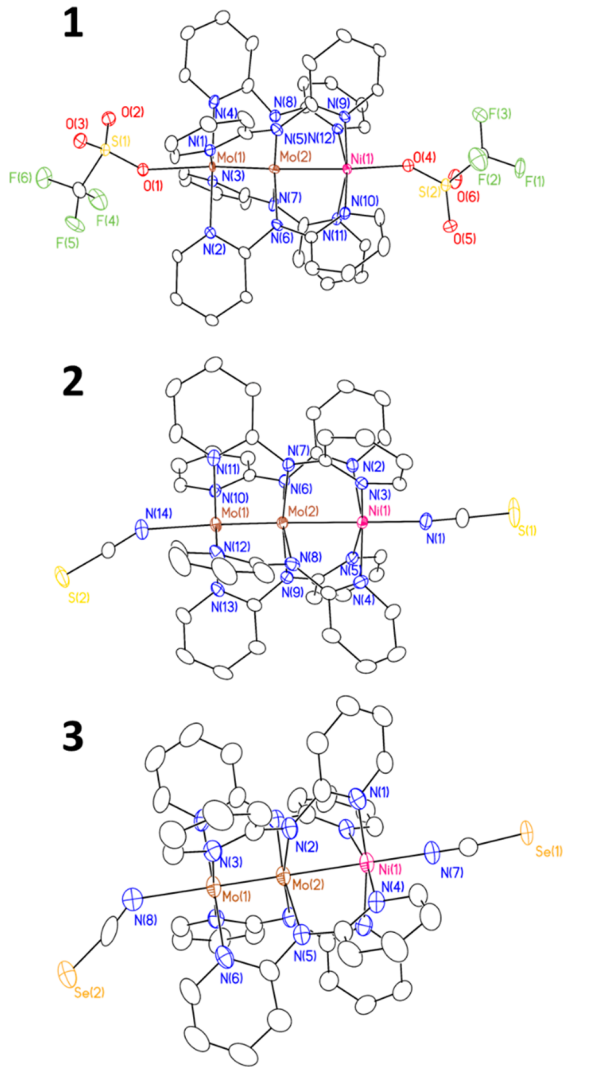

Figure 1. Crystal structures of **1**, **2**, and **3**. Ellipsoids are shown at the 50% probability level. All H atoms and molecules of solvation have been omitted for clarity. In addition, the dominant orientation in any instance of disorder is displayed.

DOI: 10.1021/acs.inorgchem.8b01331
Inorg. Chem. 2018, 57, 9354−9363

Table 1. Crystallographic Data for $Mo_2Ni(dpa)_4(OTf)_2$, $Mo_2Ni(dpa)_4(NCS)_2{\cdot}CH_2Cl_2$, and $Mo_2Ni(dpa)_4(NCSe)_2{\cdot}CH_2Cl_2$ at 100 K

	1	2	3
empirical formula	$Mo_2NiC_{42}H_{32}N_{12}S_2O_6F_6$	$Mo_2NiC_{42}H_{32}N_{14}S_2{\cdot}CH_2Cl_2$	$Mo_2NiC_{42}H_{32}N_{14}Se_2{\cdot}CH_2Cl_2$
crystal system	monoclinic	triclinic	monoclinic
space group	$P2_1/c$	$P\bar{1}$	$C2/c$
a/Å	15.67(1)	12.000(2)	18.161(4)
b/Å	17.16(2)	12.840(3)	17.381(4)
c/Å	17.82(2)	16.620(3)	15.556(3)
α/deg	90	97.73(3)	90
β/deg	107.05(1)	106.17(3)	111.19(3)
γ/deg	90	112.06(3)	90
volume/Å^3	4579(7)	2195.7(9)	4578(2)
Z	4	2	4
ρ_{calc}/(g/cm^3)	1.783	1.713	1.778
R_1,[a] wR_2[b] [$I \geq 2\sigma(I)$]	0.0438, 0.1002	0.0343, 0.0805	0.0521, 0.1194
R_1,[a] wR_2[b] [all data]	0.0471, 0.1009	0.0444, 0.0859	0.0705, 0.1301

[a] $R_1 = \Sigma||F_o| - |F_c||/\Sigma|F_o|$ [b] $wR_2 = [\Sigma[w(F_o^2 - F_c^2)^2/\Sigma[w(F_o^2)^2]]^{1/2}$, $w = 1/\sigma^2(F_o^2) + (aP)^2 + bp$ where $P = [\max(0 \text{ or } F_o^2) + 2(F_c^2)]/3$.

all presenting a linear, heterotrimetallic chain encased by the dpa ligands that wrap the molecular periphery in a helical manner. The molecular structures of compounds **1**, **2**, and **3** are shown in Figure 1.

In comparison to other Mo≡Mo quadruply bonded species supported by the dpa ligand, the Mo≡Mo bond distances for **1**, **2**, and **3** of 2.110(8), 2.1073(9), and 2.0966(8) Å, respectively (Table 1) are similar to those reported for other Mo_2M_B HEMACs that range from 2.096(2) (M = Mn) to 2.104(1) (M = Fe).[4−6,8,9] However, the Mo−Ni distances in all three complexes are remarkably short at 2.458(8)/2.47(1), 2.548(1), and 2.546(1) Å, for **1**, **2**, and **3**, respectively. To put these distances in perspective, we consider the Mo−M_B distances in $Mo_2M_B(dpa)_4Cl_2$ compounds with M_B = Cr, Mn, Fe, and Co. These distances range from 2.6170(7) Å in $Mo_2Co(dpa)_4Cl_2$ to 2.797(5) Å in the crystal structure of $Mo_2Mn(dpa)_4Cl_2$.[4−6,8] We may also make a comparison to the Mo−Ni distance in the recently reported[9] $Mo_2Ni(dpa)_4Cl_2$ which was found to be 2.525(4) Å. Indeed, **1**, **2**, **3**, and **5** present consistently short Mo−Ni distances.

Although these Mo−Ni distances are outliers among the $Mo_2M_B(dpa)_4X_2$ series, they agree well with the distance reported for the $[Ru_2Ni(dpa)_4Cl_2]^+$ ion (2.513(9) Å) synthesized by Peng and co-workers, which is described as having a (Ru_2^{5+})−Ni^{2+} electronic structure.[26,27] Additionally, **1**, **2**, **3**, and **5** may be compared to $Cr_2Ni(dpa)_4Cl_2$ reported by Nuss et al.[28] that reported a Cr−Ni bond distance of 2.585(2) Å, which is slightly shorter than the other Cr − M_B distances reported in the $Cr_2M_B(dpa)_4X_2$ series.

Mo_2M_B complexes are advantageous over Cr_2M_B complexes in that, while the electronic structure of the latter complexes are multiconfigurational and mandate a multireference computational approach,[29] the Mo_2M_B complexes may be treated satisfactorily using density functional theory (DFT) methods.[7,8,10] Crystal structure coordinates were used as starting geometries for DFT geometry optimizations and single point calculations, which allowed for additional comparison as shown in Table 2. The metal−metal bond as well as metal axial ligand distances computed for **1**, **2**, and **3** match well with experimental values. However, DFT does not accurately reflect the metal backbone to axial ligand angle (Ni/Mo−N_{NCS}−C_{NCS}) in **2**. Experimentally, these angles are observed to have a substantial bend, with metal−nitrogen−carbon angles of 151.6° and 161.1° while computationally, these values were predicted to be 177.3° and 177.4°. We attribute this discrepancy to crystal packing effects. In **3**, the Ni−N_{NCSe}−C_{NCSe} angle of the axial ligand is perfectly linear at 180.0° while the Mo−N−C angle takes a substantial bend and adopts an angle of 133.8°. Computationally, the optimized structure presents angles of 179.9°. The computational and experimental angles of **1** are in good agreement with each other.

Solution Properties. The cyclic voltammograms (CVs) for **1** and **2** in dichloromethane are shown in Figure 2. (The data for **3** are shown in Figure S3) Despite their similarity to existing HEMACs, all three compounds display distinct electrochemical behavior. These compounds all present a reversible feature, attributable to the $[Mo_2Ni]^{6+/7+}$ redox couple, at $E_{1/2}$ = −0.125 V for **1**, $E_{1/2}$ = −0.290 V for **2**, and −0.167 V for **3**. Electrochemical reversibility of this couple was established using **2**, the details of which are shown in Figures S13−S15. This redox couple has been assigned to the $Mo_2^{4+/5+}$ redox couple of the quadruple bond. We were recently able to isolate the one-electron oxidized $[Mo_2Ni(dpa)_4Cl_2]^+$ cation[9] however, this complex is not stable at room temperature. In order to access the complex, we resorted to low temperature (−78 °C) conditions for synthesis and crystallization. We attempted chemical oxidation of **2** under the same reaction conditions, using FcOTf as an oxidant, but attempted crystallization at room temperature. In this circumstance, instead of yielding a $[Mo_2Ni(dpa)_4(NCS)_2]^+$ cation, the resulting product was $[Mo_2(dpa)_3(NCS)_2]^+$ having a Mo−Mo distance of 2.580(1) Å suggestive of loss of the quadruple bond. However, there was also loss of Ni as well as one dpa ligand.[30] Thus, although the $Mo_2^{4+/5+}$ waves for **1**−**3** are reversible in an electrochemical sense, the stability of the product does not endure past the electrochemical time scale.

In the binuclear **4**, the $Mo_2^{4+/5+}$ redox event is present at $E_{1/2}$ = −0.83 V. Thus, addition of the heterometal, Ni, leads to complexes with redox potentials one-half to three-quarters of a volt higher than in the Mo_2 precursor. In comparison to other $Mo_2M_B(dpa)_4Cl_2$ compounds with M_B = Cr or Fe, **1**, **2**, and **3** present more positive redox potentials (Table 3.) We previously reported Cr≡Cr−Fe chain compounds supported by the dpa ligand in which one or both axial chloride ligands were substituted for a triflate ligand. In the monotriflate species, the triflate binds to the terminal Cr atom. Moving

DOI: 10.1021/acs.inorgchem.8b01331
Inorg. Chem. 2018, 57, 9354−9363

Table 2. Crystallographic and Computational Distances for 1, 2, 3, and 5

	Mo≡Mo, Å	Mo−Ni, Å	Mo−N_{py} (av), Å	Mo−N_a (av), Å	Ni−N_{py} (av), Å	Mo−X, Å	Ni−X, Å	Mo−L_1−L_2, deg[a]	N−L_1−L_2, deg[b]	ref
1 (major)	2.110(8)	2.485(8)	2.157[5]	2.114[2]	2.157[1]	2.364(4)	2.086(5)	150.5	149.6	this work
1 (minor)	2.14(1)	2.475(1)	2.135[5]	2.114[4]	2.1693[9]	2.317(5)	2.117(5)	151.0	149.8	this work
1 DFT	2.125	2.516	2.1828	2.1208	2.105	2.273	2.109	156.5	150.8	this work
2	2.1073(9)	2.548(1)	2.204[2]	2.131[3]	2.107[4]	2.334(2)	2.025(2)	151.6	161.1	this work
2	2.104(5)	2.546(6)	2.199[3]	2.128[3]	2.105[3]	2.333(4)	2.105(3)	150.8	162.0	23
2 DFT	2.147	2.549	2.1848	2.1225	2.1208	2.202	2.000	177.3	177.4	this work
3	2.0966(8)	2.546(1)	2.211[4]	2.121[4]	2.095[4]	2.403(6)	2.016(6)	180.0	180.0	this work
3 DFT	2.146	2.544	2.185	2.122	2.121	2.209	2.000	179.88	170.97	this work
5	2.107(2)	2.524(4)	2.115[3]	2.174[3]	2.146[3]	2.627(2)	2.394(3)	N/A	N/A	9
5 DFT	2.135	2.550	2.191	2.121	2.120	2.627	2.425	N/A	N/A	9

[a]For **1** L_1 = 0, L_2 = S. [b]For **2**, **3** L_1 = N, L_2 = C

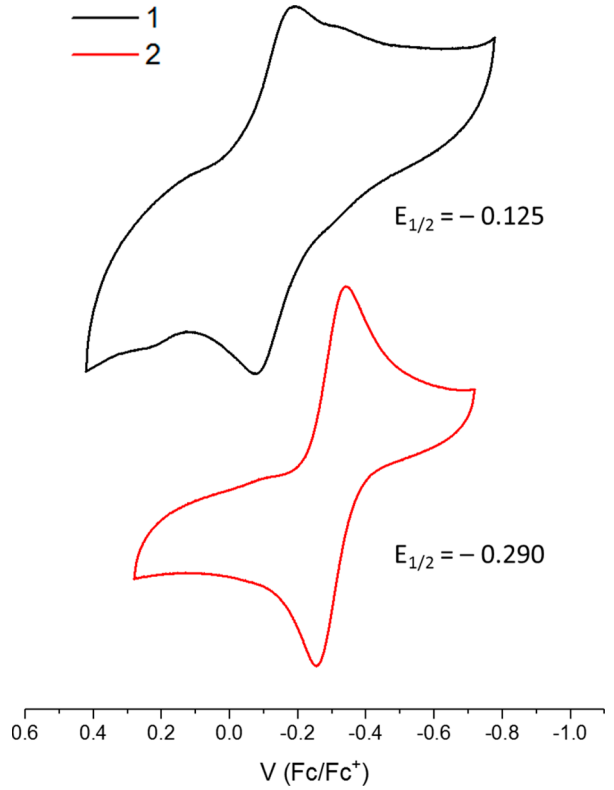

Figure 2. Cyclic voltammograms of **1** and **2** in CH_2Cl_2 with 0.1 M NBu_4PF_6 electrolyte and 1 mM substrate, scan rate 100 mV/s. For complex **1**, the lower intensity feature is attributable to degradation of the complex by air.

Table 3. Comparison of Electrochemical Data

Compound	$E_{1/2}$ (V vs Fc/Fc^+)	ref
1	−0.125	this work
2	−0.290	this work
3	−0.167	this work
5	−0.418	9
$Mo_2Cr(dpa)_4Cl_2$	−0.860	8
$Mo_2Fe(dpa)_4Cl_2$	−0.495	6
$MoWCr(dpa)_4Cl_2$	−0.910[a]	29

[a]$[MoW]^{4+/5+}$.

from the chloride to monotriflate species, the $E_{1/2}$ attributable to the $Fe^{2+/3+}$ couple was found to shift from −0.236 V to −0.050 V consistent with the fact that triflate is a weaker σ donor than chloride.[21] This work illustrates a similar trend comparing the triflate to the thiocyanate and selenocyanate ligand.

Electronic Structure. The differing colors of **1** (forest green), **2** (goldenrod), and **3** (dark brown) in CH_2Cl_2 are due to subtle differences in the three major absorption features in their electronic spectra (Figure 3). We have used our computational models of **1**, **2**, and **3** to predict the electronic transitions by TDDFT (see Figure S4). The remarkably good agreement between experimental and calculated absorption spectra serves as a strong validation for the utilized computational approach and allows us to make definitive assignments of the electronic transitions. The lowest energy transitions (band **A** in Figure 7) for all three complexes are experimentally located at 650, 663, and 665 nm for **1**, **2**, and **3**, respectively and are all attributed to Mo_2 $\delta - \delta^*$ transitions

DOI: 10.1021/acs.inorgchem.8b01331
Inorg. Chem. 2018, 57, 9354−9363

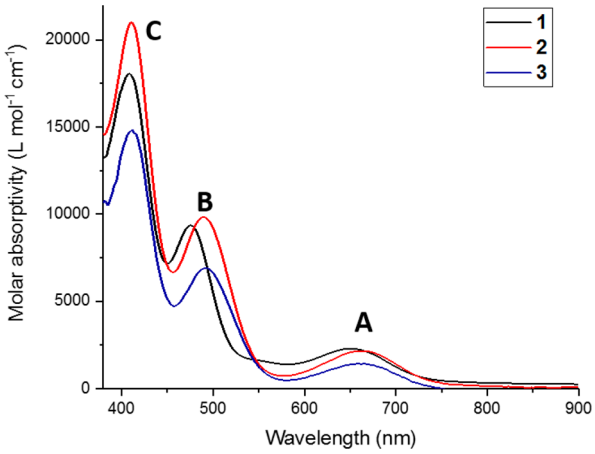

Figure 3. Experimental electronic absorbance spectra of CH_2Cl_2 solutions of **1**, **2**, and **3**.

with a degree of metal to metal charge transfer character. Compared to their experimental counterparts for transition **A**, the TDDFT calculated values of 697 nm for **1**, 726 nm for **2**, and 726 nm for **3** are slight energy underestimates of their true experimental values.

In addition, a visible energy transition **B** experimentally located at 476 nm for **1**, 477 nm for **2**, and 493 nm for **3** was matched with calculated transitions at 618, 642, and 626 nm, respectively, that are energy underestimates of their experimental values, as is common in TDDFT predictions of charge transfer transitions. Here the assignments are based more on the agreement between experimental and calculated molar absorptivities. This transition is a metal to ligand charge transfer transition from the Mo_2 δ^* orbital to a dpa π^* acceptor orbital. A complete assignment identifying all of the transitions contributing to the highest energy band **C** from the experimental spectra located at 413, 414, and 416 nm for **1**, **2**, and **3** respectively was not possible but this band is expected, based on intensity (ε = 17 900, 21 000 L, and 15 000 L mol^{-1} cm^{-1}) to also be of charge transfer transition character as well. Computationally, a major contributing transition to band **C** is a charger transfer feature located at 521 nm, 536 and 545 nm for **1**, **2**, and **3**, respectively. This transition is also a metal to ligand charge transfer transition from the Mo_2 δ^* orbital to a dpa π^* acceptor orbital with the acceptor orbital localized on the Ni-bound pyridine rings. Representative orbitals associated with these features using **2** as a model are shown in Figure 4.

In addition to TDDFT, single-point DFT calculations allow for comparison between the electronic structures of **1** − **3** and other HEMAC and EMAC compounds. The bottom four orbitals of Figure 5 derive essentially from the Mo_2 unit, having 2× π, σ, and δ symmetry (*e*, *a*, and *b* in the C_4 point group, respectively). Being filled, these orbitals contribute to the Mo≡Mo quadruple bond, though the σ symmetry orbital shows significant bonding interaction with the Ni ion as well. The next five orbitals (2*e*, 2*b*, a_{nb} and 3*b*) may be roughly assigned to the square pyramidal S = 1 Ni^{2+} center. One major perturbation to this localization of orbitals is that the a_{nb}, of σ symmetry has significant Mo contributions and can be described as Mo−Mo bonding but Mo − Ni antibonding, giving overall Mo_2Ni σ nonbonding character. Its occupation by one electron, together with the corresponding double occupation of *a*, constitute a 3*c*/3e$^-$ Mo−Mo−Ni bond akin to those originally proposed by Bénard et al. for the homometallic

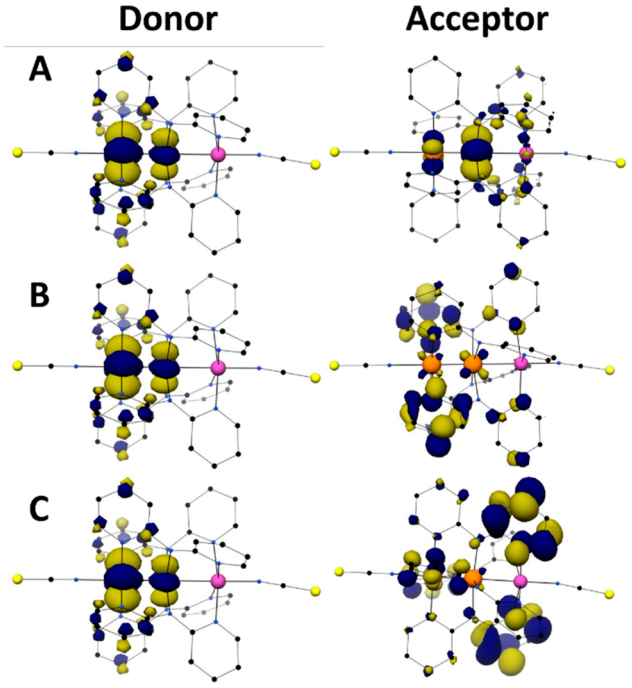

Figure 4. Representative TDDFT transitions of δ − δ^*(A) and MLCT (B, C) using **2** as a model.

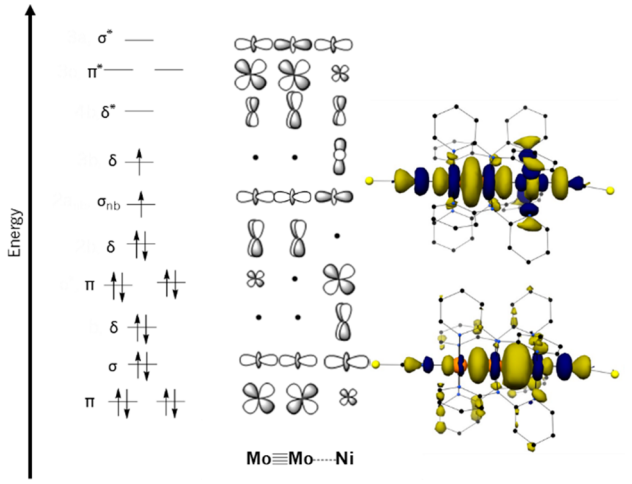

Figure 5. Qualitative MO diagram for $Mo_2Ni(dpa)_4X_2$ HEMACS based on the results of DFT calculations. The σ and σ_{nb} orbitals are shown to the right of the diagram.

$Co_3(dpa)_4Cl_2$ and $Cr_3(dpa)_4Cl_2$ species.[31−35] For the EMACs (and also for the symmetric M_A−M_B−M_A HEMACs), the D_4 symmetry gives rise to bonding and nonbonding d_{z^2} orbital combinations of differing symmetry: a_1 and a_2, respectively. The latter has a nodal plane at the position of the central atom, normal to the trimetallic axis, as seen on the left side of Chart 1. In the C_4 symmetric M_A−M_A−M_B HEMACs, all σ-symmetry orbitals belong to the *a* representation and can mix. For the σ nonbonding combination, the nodal plane lies between M_A and M_B. The compositions of these delocalized orbitals then reflect the differences in effective nuclear charge between M_A and M_B, here 28.13%:6.12%:64.75% (α) and 48.80%:12.16%:39.09% (β) for Mo_1−Mo_2−Ni for the σ bonding orbital and 33.95%:27.16%:38.90% (α) and 13.18%:21.06%:65.76% (β) for the σ nonbonding (Chart

DOI: 10.1021/acs.inorgchem.8b01331
Inorg. Chem. 2018, 57, 9354−9363

Chart 1. Comparison between the σ type Orbitals in Symmetric EMACs, Symmetric HEMACs, and Asymmetric HEMACs

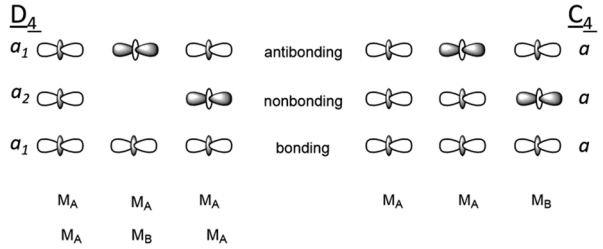

2).[36] The difference in orbital contributions between the α and β orbitals in the σ bonding contributions can be best attributed to spin polarization. To explain the difference in orbital contribution for the σ_{nb} orbitals, it is important to notice that this orbital is singly occupied and thus a difference in contribution between the α and β components is not unexpected. Similar patterns of metal atom character in the σ and σ_{nb} orbitals are seen for **1** and **3** as shown in Chart S1. Additionally, while the orbital contributions of **2** and **3** are very similar, **1** does have a noticeable difference. This is especially prominent in the α σ bonding orbitals in which **2** and **3** present nearly twice as much Ni character as **1**. This is due to σ character extending beyond the Mo_2Ni core and into the NCS or NCSe ligand (shown in the σ and σ_{nb} orbitals of **2** in Figure 5), which does not occur in triflate ligated **1**. To summarize the electronic structure of the Mo_2Ni HEMACs, a qualitative MO diagram is shown in Figure 5 in which compound **2** is used to illustrate the orbitals participating the 3c-3e$^-$ σ bond. This structure is analogous to that seen in **1**, **3**, and **5**.

Magnetic susceptibility data for **1**, **2**, and **3** are shown in Figure 6. The χT values for **1**, **2**, and **3** at 300 K, 1.02, 1.09, and 1.14 emu K mol^{-1}, respectively, agree well with the spin-only value for an $S = 1$ ground spin state (1.0 emu K mol^{-1}).[9] These values also agree with the previously reported χT value for **5** at 300 K, 1.09 emu K mol^{-1}. The data for compounds **1**, **2**, and **3** were all modeled as $S = 1$ systems including an axial zero-field splitting parameter, D. The data sets for all three compounds present a sharp downward turn in the χT plots for temperatures below 50 K, suggestive of zero field splitting. Additionally, a variable temperature/variable field (VT/VH) measurement was made for **1** in order to determine the sign of D, which is positive. The VT/VH data for **1** along with the corresponding theoretical fit are shown in Figure 7 while the overall fitting parameters for all compounds are presented in Table 4.

The fitted D values range from 5−10 cm^{-1}, in good agreement with observations for other $S = 1$ Ni^{2+} complexes.[37] For the $Mo_2Ni(dpa)_4X_2$ series, larger D values are obtained

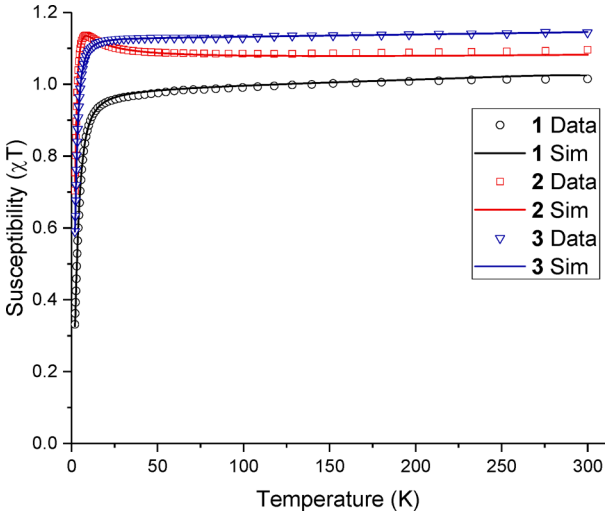

Figure 6. Magnetic susceptibility plots for **1**−**3**.

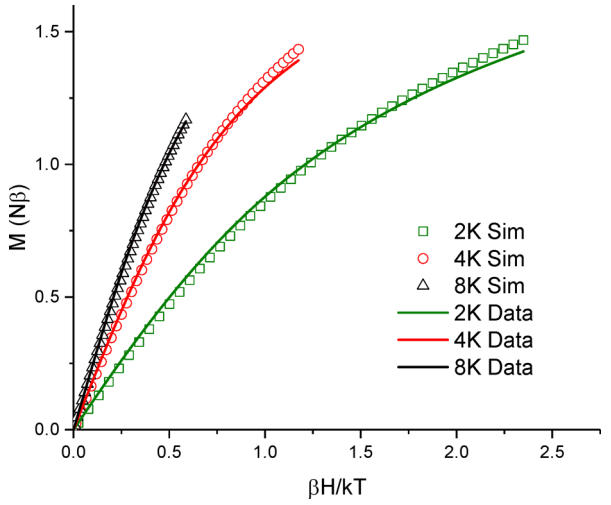

Figure 7. Variable temperature/variable field magnetization data for **1**.

when X = OTf or Cl as compared to X = NCS or NCSe. This observation is sensible as OTf and Cl are weaker field ligands as compared to NCS and NCSe and in mononuclear Ni^{2+} complexes D is inversely proportional to the energies of Ni(II) ligand-field transitions.[37] The g and D values in Table 4 deserve additional commentary. In classic perturbation theory, g values are given by $g_{\|} = g_e - 2\lambda\Lambda_{zz}$ and $g_{\perp} = g_e - 2\lambda\Lambda_{xx}$, where g_e is the free electron g-value, 2.0023, and $\lambda = -\xi/2$ where is the spin−orbit coupling constant for the complex. Here, $\Lambda_{ww} = \frac{\sum_n \langle 0|\hat{L}_w|n\rangle\langle n|\hat{L}_w|0\rangle}{E(0) - E(n)}$, which are positive for the case

Chart 2. Orbital Contributions to the σ and σ_{nb} Orbitals from the Ni and Mo Atoms[a]

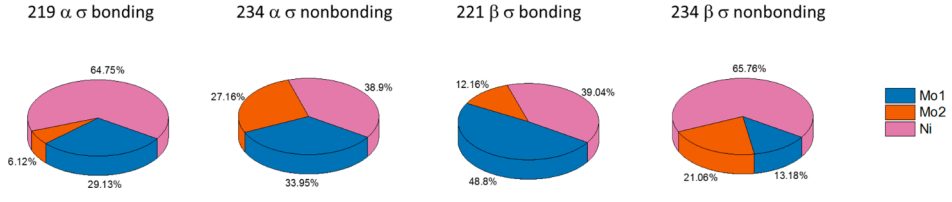

[a]Mo1 and Mo2 represent the terminal and central Mo atoms respectively.

DOI: 10.1021/acs.inorgchem.8b01331
Inorg. Chem. 2018, 57, 9354−9363

Table 4. SQUID Fitting Parameters for 1, 2, and 3, Compared to Those for Existing Mo_2Ni Complexes 5 and 5_{ox}

compound	χT at 300 K (emu K mol^{-1})	$g_{\parallel}$	$g_{\perp}$	$\lvert D\rvert$ (cm^{-1})	zJ (cm^{-1})	ref
1[a]	1.02	1.809(2)	2.297(9)	7.97(3)	0.041(5)	this work
2	1.09	1.861(1)	2.157(3)	5.587(5)	0.1834(5)	this work
3	1.14	1.8000(4)	2.2651(2)	5.394(6)	−0.0691(5)	this work
$Mo_2Ni(dpa)_4Cl_2$ (**5**)	1.09	1.817(4)	2.171(1)	9.19(3)	0.273(3)	9
$[Mo_2Ni(dpa)_4Cl_2]^+$ ($\mathbf{5}^{ox}$)	1.75	1.710(2)	2.299(3)	2.86(4)	n/a	9

[a]These values are derived from fitting of χT and reduced magnetization (variable temperature/variable field) data sets.

of Ni^{2+}. Since $\xi = -630\ cm^{-1}$ for the free Ni^{2+} ion, values of g_z and g_x are all expected to be greater than 2. Clearly, the g_z values in Table 4 do not follow this expectation. Further considering the relationship between D and g anisotropy, $\Delta g = g_{\parallel} - g_{\perp}$, for mononuclear Ni $^{2+}$ complexes, namely, $D = \frac{1}{2}\lambda(\Delta g)$, the D values we observe would predict values of Δg that are too small by an order of magnitude from what we observe. These observations lead to the conclusion that electron delocalization along the Ni^{2+} and the heavier Mo^{2+} ions in these complexes has a major contribution to the g anisotropy. In particular, g_z, mainly affected by $|d_{z^2}\rangle$, is less that g_e as would be much more typical of the g values of a Mo^{2+} ion. Thus, the magnetic data for **1**−**3** and **5** strongly support the result, seen in our DFT calculations, that the Ni^{2+} d_{z^2} unpaired electron is highly delocalized covalently with the Mo^{2+} ions.

SUMMARY

In previous work, we have made a magnetic comparison between $CrCrCo(dpa)_4Cl_2$ and $MoMoCo(dpa)_4Cl_2$ and found that the $Mo_2(dpa)_4$ "ligand" provides a weaker ligand field to Co^{2+} than does the $Cr_2(dpa)_4$ "ligand."[4] It is therefore surprising that, synthetically, we find demetalation from the $Cr_2(dpa)_4$ ligand to be more facile than from the $Mo_2(dpa)_4$ "ligand." We attribute this effect to the stronger $3c/3e^-$ interaction involving the more diffuse orbitals of Mo than Cr.

The ability to cleanly and easily substitute the axial ligands of $Mo_2Ni(dpa)_4(OTf)_2$ suggests that other $Mo_2M(dpa)_4(OTf)_2$ HEMACs may behave in a similar way. This, in turn, will allow for additional exploration and tuning of the properties of HEMAC complexes. DFT calculations for all three compounds reported here suggest that the $3c/3e^-$ σ bond helps support the $Mo_2Ni(dpa)_4X_2$ complexes and greatly enhances the g anisotropy of the compounds. This motif is present along other $Mo_2M(dpa)_4X_2$ complexes providing further impetus to explore their axial ligand substitution chemistry as well.

EXPERIMENTAL SECTION

Materials and Methods. All reactions were carried out under a dry N_2 atmosphere using Schlenk techniques and glovebox methods. Hexanes, acetonitrile, tetrahydrofuran, and diethyl ether were purified using a Vacuum Atmospheres solvent purification system and dichloromethane was freshly distilled under an N_2 atmosphere over CaH_2 prior to use. Naphthalene was purchased from Sigma-Aldrich and sublimed prior to use. The ligand Hdpa was purchased from TCI and recrystallized from hot hexanes prior to use. $Ni(OTf)_2$, NaNCS, and KNCSe were purchased from Strem Chemicals. $Ni(OTf)_2$ was used as received while NaNCS and KNCSe were dried under vacuum at 40 °C overnight prior to use. Elemental analysis was carried out by Midwest Microlabs, LLC inc., Indianapolis, IN. IR spectra were taken on a BRUKER TENSOR 27 FTIR spectrometer using an attenuated total reflectance (ATR) adapter. Cyclic voltammograms (CVs) for **1** and **2** were taken on a BASI Epsilon EC potentiostat while **3** was taken on a BioLogic SP200 EC potentiostat. All CVs were obtained using CH_2Cl_2 solutions with 0.1 M NBu_4PF_6 and 1 mM substrate. The electrodes were as follows: glassy carbon (working), Pt wire (auxiliary), and Ag/Ag^+ in CH_3CN (reference). The potentials were referenced against the ferrocene/ferrocenium redox couple by external addition of ferrocene. Variable temperature magnetic susceptibility measurements of crystalline samples of **1**, **2**, and **3** were recorded at the University of Wisconsin-Madison on a SQUID Magnetometer (MPMS 3, Quantum Design) in the temperature range 2−300 K with an applied field of 0.1 T. Variable temperature/variable field measurements of a crystalline sample of **1** were also collected on the same magnetometer at 2, 4, and 8 K at a field ranging from 0.1 to 7 T. Experimental susceptibility and magnetization data were corrected for the underlying diamagnetism using Pascal's constants[38] and for the temperature independent paramagnetism contributions. The data were modeled using the program PHI.[39] ^1H and ^{13}C NMR spectra were obtained on a 500 MHz Bruker Avance III.

Crystallography. Crystallographic data were measured at the Molecular Structure Laboratory of the Chemistry Department of the University of Wisconsin−Madison. Crystals were selected under oil under ambient conditions and attached to the tip of a MiTeGen MicroMount. Each crystal was mounted under a stream of cold nitrogen at 100(1) K and centered in the X-ray beam using a video camera. The crystal evaluation and data collection were performed on a Bruker Quazar SMART APEXII diffractometer with Mo Kα (λ = 0.71073 Å) radiation with a detector to crystal distance of 5.0 cm. The data were collected using a routine to survey the entire sphere of reciprocal space, and were indexed by the SMART program.[40] The structures were solved using direct methods and refined by least-squares refinement on F^2 followed by difference Fourier synthesis.[41] All hydrogen atoms were included in the final structure factor calculation at idealized positions and were allowed to ride on the neighboring atoms with relative isotropic displacement coefficients.

There was 56% positional metal atom disorder in **1** with the Mo≡Mo−Ni unit ordered in two opposing orientations. The central nitrogen atoms of the dpa ligand were also found to be disordered and were split with occupancies matching the positional metal atom disorder. This nitrogen atom disorder had not been necessary in the refinement of previously synthesized HEMACs. We hypothesize that the two sets of N atom positions reflect the propensity for the Mo≡Mo bond to confer low N−Mo−Mo−N torsion angles, due to the Mo−Mo δ bond. The metal atoms and nitrogen atoms in **2** and **3** are ordered; for **2**, the axial NCS ligand appended to the terminal Mo was also positionally disordered. Complex **3** crystallized as a two component twin and presented positional disorder of one axial NCSe ligand in addition to positional disorder of the selenium atom of the other ligand.

Computational Methods. The initial coordinates for the calculations were obtained from the crystallographic data for **1**, **2**, and **3** with the solvent molecules of crystallization removed and the dominant orientation for any disorder utilized. All calculations were carried out using the program ORCA version 3.0.3.[42] The BP86 exchange-correlation functional[43,44] including the ZORA approximation was used.[45] The Stuttgart-Dresden effective core potential (ECP), def2-SD,[46] was used along with the valence basis sets def2-TZVP and density fitting basis set def2-TZVP/J for Mo atoms.[47,48] The def2-TZVP basis set and def2-TZVP/J auxiliary basis set was used for Ni.[49,50] The def2-SVP basis set and def2-SVP/J density fitting basis set were used for all other atoms. Tight optimization and tight self-consistent field convergence criteria were employed along

DOI: 10.1021/acs.inorgchem.8b01331
Inorg. Chem. 2018, 57, 9354−9363

with grid4 for all calculations. Frequency calculations were performed following geometry optimizations to ensure the structures were at local minima. Löwdin population analysis was done to determine orbital populations.[51,52] Visualizations were carried out with the UCSF Chimera package.[53] Symmetry labels presented in the molecular orbital diagram were assigned by inspection to conform with the idealized C_4 point group.

Synthetic Methods. *Kdpa.* The ligand Hdpa (3.30 g, 19.27 mmol) and $KN(TMS)_2$ (3.86g, 19.38 mmol)) were separately dissolved in minimal quantities of diethyl ether. Dropwise, the $KN(TMS)_2$ solution was added to the Hdpa solution affording a milky off-white precipitate. The reaction mixture was allowed to stir at room temperature for 30 min before being filtered and the solid was washed with washed with 2 × 30 mL of additional diethyl ether. The off-white powder was collected and dried under vacuum (3.38 g, 83.8%). ^{1}H NMR (500 MHz, THF-d_8, assignments in Figure 8): δ (ppm) 6.24 (ddd, J = 6.65, 5.05, 1.07 Hz, 2H, H2), 7.12 (ddd, J = 8.70, 6.82, 2.14 Hz, 2H, H3), 7.31 (ddd, J = 8.76, 1.04 Hz, 2H, H4), 7.94 (ddd, J = 5.01, 2.16, 0.91 Hz, 2H, H1), ^{13}C NMR (500 MHz, d_8 THF): δ (ppm) 109.43, 112.77, 134.73, 147.25, 163.03. Anal. Calcd for $KC_{10}N_3H_8$: C, 57.38; H, 3.85; N, 20.07. Found: C, 56.62; H, 3.82; N, 20.07. IR (ATR, cm^{-1}): 1746 w, 1602 m, 1566 s, 1463 s, 1427 s, 1376 s, 1340 w, 1310 m, 1277 w, 1231 m, 1157 m, 1056 m, 1030 m, 861 w, 768 m, 750 m, 740 m, 692 w, 666 w, 636 s.

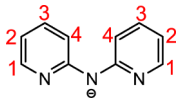

Figure 8. Kdpa with numbers for proton assignment in ^{1}H NMR spectrum.

*$Mo_2(dpa)_4$ (**4**).* Canary yellow $Mo_2(OAc)_4$ (2.10 g, 4.91 mmol) and off-white Kdpa (4.20 g, 20.01 mmol) were combined in a Schlenk flask. Upon addition of 100 mL of THF, the contents of the flask turned a brick red color. The reaction was allowed to proceed under refluxing conditions overnight during which time a dark red precipitate formed. This solid was isolated via filtration and washed with 3 × 30 mL MeOH, and 3 × 30 mL diethyl ether. The red powder was then collected and dried under vacuum (3.63g, 84.9%) The IR spectrum was identical to that previously reported.[4]

*$Mo_2Ni(dpa)_4(OTf)_2$ (**1**).* Solid brick-red $Mo_2(dpa)_4$ (0.446 g, 0.511 mmol) and $Ni(SO_3CF_3)_2$ (0.282 g, 0.790 mmol) were combined with naphthalene (5 g) in a Schlenk flask. The flask was placed in a sandbath that had been preheated to 200 °C and stirred for 2 h during which time the reaction mixture became dark green in color. After cooling to room temperature, the solidified reaction mixture was washed with hot hexanes (4 × 40 mL). The residual dark solid was dried under vacuum and subsequently extracted with dichloromethane (30 mL). The dark green extract was then layered with hexanes (70 mL). Dark colored X-ray quality blocks of **1** were obtained after 3 days. Yield: 212 mg, 33.7%. ^{1}H NMR (500 MHz, CD_2Cl_2): δ (ppm) 0.51 (s), 6.75 (s), 9.64 (s), 12.49 (s), 16.47 (s), 30.15 (s). Anal. Calcd for $Mo_2Ni(dpa)_4(SO_3CF_3)_2\cdot CH_2Cl_2$: C, 39.29; H, 2.61; N, 12.79. Found: C, 39.55; H, 2.71; N, 12.72. IR (ATR, cm^{-1}): 1600 m, 1578 s, 1478 w, 1453 m, 1429 s, 1370 s, 1302 s, 1284 w, 1250 w, 1174 m, 1056 m, 1015 w, 986 w, 878 w, 852 w, 835 w, 768 s, 754 s, 745 w, 728 m, 698 m, 662 m, 642 m, 618 w.

*$Mo_2Ni(dpa)_4(NCS)_2$ (**2**).* Green **1** (64.8 mg, 0.0600 mmol) was dissolved in 10 mL of CH_2Cl_2 while a 30.3 mM solution of NaNCS in CH_3CN was separately prepared. The solution of **1** was cooled to 0 °C in an ice bath and 3.2 mL of the NaNCS solution was added to it dropwise over the course of several minutes. The resulting solution turned from forest green to goldenrod and was subsequently warmed to room temperature. The solvent was then removed under vacuum and the resulting brown powder was dissolved in 10 mL of CH_2Cl_2 and filtered over a medium porosity filter frit. The brown solution was layered with diethyl ether (40 mL). Dark block X-ray quality crystals of **2** grew after 1 week. Crystalline yield: 24.8 mg, 45%. Following filtration, the filtrate may be concentrated again to afford **2** as a powder in higher yields. ^{1}H NMR (500 MHz, CD_2Cl_2): δ (ppm) 0.35 (s), 6.63 (s), 7.27 (s), 8.63 (s), 12.62 (s), 31.64 (s). Anal. Calcd for $Mo_2Ni(dpa)_4(NCS)_2\cdot CH_2Cl_2$: C, 45.61; H, 3.03; N, 17.32. Found: C, 45.90; H, 3.31; N, 16.73. IR (ATR, cm^{-1}): 2063 m, 1602 m, 1592 m, 1550 w, 1456 s, 1420 s, 1359 s, 1308 s, 1279 w, 1150 m, 1051 m, 1017 w, 964 w, 927 w, 894 m, 816 m, 770 s, 761 s, 740 w, 668 m, 640 m.

*$Mo_2Ni(dpa)_4(NCSe)_2$ (**3**).* Green **1** (28.6 mg, 0.0233 mmol) was dissolved in 25 mL of CH_2Cl_2 while a 22.6 mM solution of KNCSe in CH_3CN was separately prepared. The solution of **1** was cooled to 0 °C in an ice bath to which 2.06 mL of the KNCSe solution was added dropwise over the course of several minutes. The solution turned from forest green to brown and was subsequently warmed to room temperature. The solvent was then removed under vacuum and the resulting brown powder was dissolved in 15 mL of CH_2Cl_2 and filtered over a medium porosity filter frit. The brown solution was layered with diethyl ether (40 mL). Dark needle−block X-ray quality crystals of **3** grew after 3 days. Crystalline yield: 11.66 mg, 44.0%. Anal. Calcd for $Mo_2Ni(dpa)_4(NCSe)_2\cdot CH_2Cl_2$: C, 42.12; H, 2.79; N, 15.99. Found: C, 41.76; H, 2.87; N, 16.40. IR (ATR, cm^{-1}): 2075 m, 2009 m, 1602 m, 1593 m, 1562 m, 1474 m, 1458 s, 1420 s, 1349 s, 1307 s, 1280 w, 1155 m, 1059 m, 1015 w, 880 m, 857 m, 810 m, 765 s, 750 w, 738 w, 690 m.

■ ASSOCIATED CONTENT

Supporting Information

The Supporting Information is available free of charge on the ACS Publications website at DOI: 10.1021/acs.inorgchem.8b01331.

Additional orbital figures, Cartesian coordinates, crystallographic details and other spectroscopic details (PDF)

Accession Codes

CCDC 1843431−1843434 contain the supplementary crystallographic data for this paper. These data can be obtained free of charge via www.ccdc.cam.ac.uk/data_request/cif, or by emailing data_request@ccdc.cam.ac.uk, or by contacting The Cambridge Crystallographic Data Centre, 12 Union Road, Cambridge CB2 1EZ, UK; fax: +44 1223 336033.

■ AUTHOR INFORMATION

Corresponding Author

*(J.F.B.) E-mail berry@chem.wisc.edu.

ORCID

Jill A. Chipman: 0000-0002-3243-8766

John F. Berry: 0000-0002-6805-0640

Funding

This work was supported in part by the National Science Foundation (CHE-1669994).

Notes

The authors declare no competing financial interest.

■ ACKNOWLEDGMENTS

We are grateful to the National Science Foundation for support via Grant CHE-1669994. In addition, Computational Facilities used to support this work were supported by the NSF under Grant CHE-0840494. The NMR spectrometer used is supported under a gift from the Bender Fund. J.F.B. additionally thanks the Alexander von Humboldt Foundation and Prof. Karsten Meyer for facilitating some preliminary experiments to those reported here. J.A.C. acknowledges Dr. Brian Dolinar for his crystallographic advice, Dr. Tzuhsiung

DOI: 10.1021/acs.inorgchem.8b01331
Inorg. Chem. 2018, 57, 9354−9363

Yang for his computational insight, and Manar Alherech for his NMR assistance.

REFERENCES

(1) Nippe, M.; Berry, J. F. Introducing a Metal−Metal Multiply Bonded Group as an "Axial Ligand" to Iron: Synthetic Design of a Linear Cr≡Cr···Fe Framework. *J. Am. Chem. Soc.* **2007**, *129*, 12684−12685.

(2) Rohmer, M.-M.; Liu, I. P.-C.; Lin, J.-C.; Chiu, M.-J.; Lee, C.-H.; Lee, G.-H.; Bénard, M.; López, X.; Peng, S.-M. Structural, Magnetic, and Theoretical Characterization of a Heterometallic Polypyridylamide Complex. *Angew. Chem., Int. Ed.* **2007**, *46*, 3533−3536.

(3) Berry, J. F.; Cotton, F. A.; Daniels, L. M.; Murillo, C. A. A Trinickel Dipyridylamido Complex with Metal−Metal Bonding Interaction: Prelude to Polynickel Molecular Wires and Devices? *J. Am. Chem. Soc.* **2002**, *124*, 3212−3213.

(4) Nippe, M.; Victor, E.; Berry, J. F. Do Metal−Metal Multiply-Bonded "Ligands" Have a trans Influence? Structural and Magnetic Comparisons of Heterometallic Cr≡Cr···Co and Mo≡Mo···Co Interactions. *Eur. J. Inorg. Chem.* **2008**, *2008*, 5569−5572.

(5) Nippe, M.; Wang, J.; Bill, E.; Hope, H.; Dalal, N. S.; Berry, J. F. Crystals in Which Some Metal Atoms are More Equal Than Others: Inequalities From Crystal Packing and Their Spectroscopic/Magnetic Consequences. *J. Am. Chem. Soc.* **2010**, *132*, 14261−14272.

(6) Nippe, M.; Bill, E.; Berry, J. F. Group 6 Complexes with Iron and Zinc Heterometals: Understanding the Structural, Spectroscopic, and Electrochemical Properties of a Complete Series of M≡M···M′ Compounds. *Inorg. Chem.* **2011**, *50*, 7650−7661.

(7) Brogden, D. W.; Berry, J. F. Heterometallic Second-Row Transition Metal Chain Compounds in Two Charge States: Syntheses, Properties, and Electronic Structures of $[Mo{\equiv}Mo{-}Ru]^{6+/7+}$ Chains. *Inorg. Chem.* **2015**, *54*, 7660−7665.

(8) Brogden, D. W.; Christian, J. H.; Dalal, N. S.; Berry, J. F. Completing the series of Group VI heterotrimetallic $M_2Cr(dpa)_4Cl_2$ (M_2 = Cr_2, Mo_2, MoW and W_2) compounds and investigating their metal−metal interactions using density functional theory. *Inorg. Chim. Acta* **2015**, *424*, 241−247.

(9) Chipman, J. A.; Berry, J. F. Extraordinarily Large Ferromagnetic Coupling ($J \geq 150$ cm^{-1}) by Electron Delocalization in a Heterometallic Mo≡Mo−Ni Chain Complex. *Chem. - Eur. J.* **2018**, *24*, 1494−1499.

(10) Brogden, D. W.; Berry, J. F. Heterometallic Multiple Bonding: Delocalized Three-Center σ and π Bonding in Chains of 4d and 5d Transition Metals. *Inorg. Chem.* **2014**, *53*, 11354−11356.

(11) Clérac, R.; Cotton, F. A.; Dunbar, K. R.; Lu, T.; Murillo, C. A.; Wang, X. New Linear Tricobalt Complex of Di(2-pyridyl)amide (dpa), $[Co_3(dpa)_4(CH_3CN)_2][PF_6]_2$. *Inorg. Chem.* **2000**, *39*, 3065−3070.

(12) Clerac, R.; Cotton, F. A.; Daniels, L. M.; Dunbar, K. R.; Murillo, C. A.; Wang, X. Structural and magnetic properties of $Co_3(dpa)_4Br_2$. *Dalton Trans.* **2001**, 386−391.

(13) Clérac, R.; Cotton, F. A.; Jeffery, S. P.; Murillo, C. A.; Wang, X. Compounds with Symmetrical Tricobalt Chains Wrapped by Dipyridylamide Ligands and Cyanide or Isothiocyanate Ions as Terminal Ligands. *Inorg. Chem.* **2001**, *40*, 1265−1270.

(14) Berry, J. F.; Albert Cotton, F.; Murillo, C. A. Making connections with molecular wires: extending tri-nickel chains with axial cyanide, dicyanamide, and phenylacetylide ligands. *Dalton Trans.* **2003**, 3015−3021.

(15) Berry, J. F.; Cotton, F. A.; Lu, T.; Murillo, C. A.; Roberts, B. K.; Wang, X. Molecular and Electronic Structures by Design: Tuning Symmetrical and Unsymmetrical Linear Trichromium Chains. *J. Am. Chem. Soc.* **2004**, *126*, 7082−7096.

(16) Berry, J. F.; Cotton, F. A.; Murillo, C. A. A Trinuclear EMAC-Type Molecular Wire with Redox-Active Ferrocenylacetylide "Alligator Clips" Attached. *Organometallics* **2004**, *23*, 2503−2506.

(17) Berry, J. F.; Cotton, F. A.; Murillo, C. A.; Roberts, B. K. An Efficient Synthesis of Acetylide/Trimetal/Acetylide Molecular Wires. *Inorg. Chem.* **2004**, *43*, 2277−2283.

(18) Cotton, F. A.; Murillo, C. A.; Walton, R. A. *Multiple Bonds between Metal Atoms* **2005**, 1.

(19) Cotton, F. A.; Murillo, C. A.; Wang, Q. Symmetrical linear Co_3^{6+} chains cocooned by two polypyridylamide ligands: How do they compare to open chains? *Inorg. Chim. Acta* **2010**, *363*, 4175−4180.

(20) Li, H.; Yan, J.; Xu, Y. Y.; Gao, W. G.; Lee, G.-H.; Peng, S.-M. Hydrogen-bonded assemblies of trinuclear metal string complexes. *J. Coord. Chem.* **2007**, *60*, 2731−2738.

(21) Nippe, M.; Turov, Y.; Berry, J. F. Remote Effects of Axial Ligand Substitution in Heterometallic Cr≡Cr···M Chains. *Inorg. Chem.* **2011**, *50*, 10592−10599.

(22) Turov, Y.; Berry, J. F. Synthesis, characterization and thermal properties of trimetallic N_3-Cr≡Cr···M-N_3 azide complexes with M = Cr, Mn, Fe, and Co. *Dalton Trans.* **2012**, *41*, 8153−8161.

(23) Chang, W.-C.; Chang, C.-W.; Sigrist, M.; Hua, S.-A.; Liu, T.-J.; Lee, G.-H.; Jin, B.-Y.; Chen, C.-h.; Peng, S.-M. Nonhelical heterometallic $[Mo_2M(npo)_4(NCS)_2]$ string complexes (M = Fe, Co, Ni) with high single-molecule conductance. *Chem. Commun.* **2017**, *53* (63), 8886−8889.

(24) It is important to note that axial ligand substitution studies have not been reported for $Cr_2Ni(dpa)_4C_{l2}$ to fully understand the significance of the Ni atom in the chain in addition to moving to a Mo_2 core.

(25) Hurley, T. J.; Robinson, M. A. Nickel(II)-2,2′-dipyridylamine system. I. Synthesis and stereochemistry of the complexes. *Inorg. Chem.* **1968**, *7*, 33−38.

(26) Huang, G.-C.; Bénard, M.; Rohmer, M.-M.; Li, L.-A.; Chiu, M.-J.; Yeh, C.-Y.; Lee, G.-H.; Peng, S.-M. $Ru_2M(dpa)_4Cl_2$ (M = Cu, Ni): Synthesis, Characterization, and Theoretical Analysis of Asymmetric Heterometal String Complexes of the Dipyridylamide Family. *Eur. J. Inorg. Chem.* **2008**, *2008*, 1767−1777.

(27) The neutral $Ru_2Ni(dpa)_4Cl_2$ molecule was studied crystallographically; however, metal atom disorder was so severe that the reported anomalous Ru−Ni distance is fixed to an unreliable value.

(28) Aydin-Cantürk, D.; Nuss, H. Synthesis, Structure Determination, and Magnetic Properties of the New Heterometallic Chain Compound CrCrNi(di-2,2′-pyridylamido)$_4Cl_2$·Et_2O. *Z. Anorg. Allg. Chem.* **2011**, *637*, 543−546.

(29) Arcisauskaite, V.; Spivak, M.; McGrady, J. E. Structure and bonding in trimetallic arrays containing a Cr−Cr quadruple bond: A challenge to density functional theory. *Inorg. Chim. Acta* **2015**, *424*, 293−299.

(30) Unit cell parameters: *a*/Å, 11.474(7); *b*/Å, 13.311(9); *c*/Å, 13.971(8); α/deg, 80.95(1); β/deg, 88.202(7); γ/deg, 74.25(1); volume/Å^3, 2028(2); Z = 2. $Mo_2(C_{10}H_8N_3)_3(NCS)_2(SO_3CF_3)$·$CH_2Cl_2$

(31) Rohmer, M.-M.; Bénard, M. Bond Stretch Isomerism Still Elusive in Linear Trimetallic Complexes. DFT Calculations on Co_3(dipyridylamine)$_4Cl_2$. *J. Am. Chem. Soc.* **1998**, *120*, 9372−9373.

(32) Benbellat, N.; Rohmer, M.-M.; Benard, M. Electronic origin of the structural versatility in linear trichromium complexes of dipyridylamide. *Chem. Commun.* **2001**, 2368−2369.

(33) Rohmer, M.-M.; Strich, A.; Bénard, M.; Malrieu, J.-P. Metal−Metal Bond Length Variability in Co_3(dipyridylamide)$_4Cl_2$: Bond-Stretch Isomerism, Crystal Field Effects, or Spin Transition Process? A DFT Study. *J. Am. Chem. Soc.* **2001**, *123*, 9126−9134.

(34) Rohmer, M.-M.; Benard, M. Bond-stretch Isomerism in Strained Inorganic Molecules and in Transition Metal Complexes: a Revival? *Chem. Soc. Rev.* **2001**, *30*, 340−354.

(35) Rohmer, M.-M.; Bénard, M. Structural Versatility in Polyoxometalates and in Some Linear Trimetallic Complexes: An Electronic Interpretation. *J. Cluster Sci.* **2002**, *13*, 333−353.

(36) Values are derived from the Löwdin analysis of the wave function

(37) Boča, R. Zero-field splitting in metal complexes. *Coord. Chem. Rev.* **2004**, *248*, 757−815.

(38) Bain, G. A.; Berry, J. F. Diamagnetic Corrections and Pascal's Constants. *J. Chem. Educ.* **2008**, *85*, 532.

DOI: 10.1021/acs.inorgchem.8b01331
Inorg. Chem. 2018, 57, 9354−9363

(39) Chilton, N. F.; Anderson, R. P.; Turner, L. D.; Soncini, A.; Murray, K. S. PHI: A powerful new program for the analysis of anisotropic monomeric and exchange-coupled polynuclear d- and f-block complexes. *J. Comput. Chem.* **2013**, *34*, 1164−1175.
(40) *SMART*; Bruker-AXS, Madison, WI, 2009.
(41) Dolomanov, O. V; Bourhis, L. J; Gildea, R. J; Howard, J. A. K; Puschmann, H. OLEX 2: a complete structure solution, refinement and analysis program. *J. Appl. Crystallogr.* **2009**, *42*, 339−341.
(42) Neese, F. The ORCA program system. *Wiley Interdisciplinary Reviews: Computational Molecular Science* **2012**, *2* (1), 73−78.
(43) Becke, A. D. Density-functional exchange-energy approximation with correct asymptotic behavior. *Phys. Rev. A: At., Mol., Opt. Phys.* **1988**, *38*, 3098−3100.
(44) Perdew, J. P.; Yue, W. Accurate and simple density functional for the electronic exchange energy: Generalized gradient approximation. *Phys. Rev. B: Condens. Matter Mater. Phys.* **1986**, *33*, 8800−8802.
(45) Pantazis, D. A.; Chen, X.-Y.; Landis, C. R.; Neese, F. All-Electron Scalar Relativistic Basis Sets for Third-Row Transition Metal Atoms. *J. Chem. Theory Comput.* **2008**, *4*, 908−919.
(46) Andrae, D.; Haussermann, U.; Dolg, M.; Stoll, H.; Preuss, H. Energy-Adjusted ab initio Pseudopotentials for the Second and Third Row Transition Elements. *Theor. Chem. Acc.* **1990**, *77*, 123−141.
(47) Weigend, F.; Ahlrichs, R. Balanced basis sets of split valence, triple zeta valence and quadruple zeta valence quality for H to Rn: Design and assessment of accuracy. *Phys. Chem. Chem. Phys.* **2005**, *7*, 3297−3305.
(48) Weigend, F. Accurate Coulomb-fitting basis sets for H to Rn. *Phys. Chem. Chem. Phys.* **2006**, *8*, 1057−1065.
(49) Eichkorn, K.; Treutler, O.; Öhm, H.; Häser, M.; Ahlrichs, R. Auxiliary basis sets to approximate Coulomb potentials. *Chem. Phys. Lett.* **1995**, *240*, 283−290.
(50) Eichkorn, K.; Weigend, F.; Treutler, O.; Ahlrichs, R. Auxiliary basis sets for main row atoms and transition metals and their use to approximate Coulomb potentials. *Theor. Chem. Acc.* **1997**, *97*, 119−124.
(51) Löwdin, P. O. On the Non-Orthogonality Problem Connected with the Use of Atomic Wave Functions in the Theory of Molecules and Crystals. *J. Chem. Phys.* **1950**, *18*, 365−375.
(52) Löwdin, P. O. On the Nonorthogonality Problem. *Adv. Quantum Chem.* **1970**, *5*, 185−199.
(53) Pettersen, E. F.; Goddard, T. D.; Huang, C. C.; Couch, G. S.; Greenblatt, D. M.; Meng, E. C.; Ferrin, T. E. UCSF Chimera—A visualization system for exploratory research and analysis. *J. Comput. Chem.* **2004**, *25*, 1605−1612.

DOI: 10.1021/acs.inorgchem.8b01331
Inorg. Chem. 2018, 57, 9354−9363